Article

Coordinated PSO-ANFIS-Based 2 MPPT Control of Microgrid with Solar Photovoltaic and Battery Energy Storage System

Siddaraj SIddaraj [1,*] , Udaykumar R. Yaragatti [2] and Nagendrappa Harischandrappa [2]

1   Department of Electrical and Electronics Engineering, Manipal Institute of Technology,
    Manipal Academy of Higher Education, Manipal 576104, India
2   Department of Electrical and Electronics Engineering, National Institute of Technology Karnataka,
    Mangalore 575025, India; udaya@nitk.ac.in (U.R.Y.); nagendrappa@nitk.edu.in (N.H.)
*   Correspondence: siddaraj.u@manipal.edu

Abstract: The microgrid is a group of smaller renewable energy sources (REs), which act in a coordinated manner to provide the required amount of active power and additional services when required. This article proposes coordinated power management for a microgrid with the integration of solar PV plants with maximum power point tracking (MPPT) to enhance power generation and conversion using a hybrid MPPT method based on particle swarm optimization-adaptive neuro-fuzzy inference system (PSO-ANFIS) to acquire rapid and maximum PV power along with battery energy storage control to maintain the stable voltage and frequency (V-f) of an isolated microgrid. In addition, it is proposed to provide active and reactive power (P-Q) regulation for the grid connected. The approach used provides more regulation due to the least root mean square error (RMSE), which improves photovoltaic (PV) potential extraction. The comparison results of the PSO-ANFIS and P&O controllers of the MPPT and the controller of the energy storage devices combined with the V-f (or P-Q) controller of the inverter all show effective coordination between the control systems. This is the most important need for contemporary microgrids, considering the potential of changing irradiance in the grid following mode, the grid forming mode under an island scenario, and back-to-grid synchronization. With the test model, the islanded and grid-islanded-grid connected modes are investigated separately. The results demonstrate conclusively that the proposed strategies are effective. To run the simulations, MATLAB and SimPowerSystems are utilized.

Keywords: microgrid; photovoltaic (PV) system; PSO-ANFIS MPPT; PQ power control; battery energy storage system (BESS); droop control

1. Introduction

The microgrid is a network of dispersed micro resources, storage devices, and demands that work as a single, autonomous, controllable system able to supply both electricity and heat to the service area [1]. The micro resources of a microgrid consist of minor devices with less than 1 MW of electricity and a power electronic (PE) interface. The distribution power supply is connected to the most prevalent non-conventional resources, such as solar photovoltaic systems, fuel cells, microturbines, storage devices, etc.

The micro source controllers in a microgrid connect the storage and micro sources to the feeders, while the control system manages coordination amongst all sources [2]. The circuit breakers establish the point of common coupling (PCC), where the microgrid is connected to the electrical grid. When the microgrid is associated with the grid, the grid maintains its ability to operationally regulate frequency and voltage, but the microgrid continues to supply PCC's loads and acts as a PQ bus. For the microgrid to regulate its frequency and voltage in an isolated mode, it must provide all its power without much assistance from the grid. In this way, the microgrid performs like a power-voltage bus. Micro-resource controllers are present both locally and globally to coordinate and control

the various modes of operation and resource management. On the inverter side droop, the controller is switched to share power among distributed generators in an autonomous mode and back to grid mode as the PQ controller. This controller is feasible to manage the microgrid's frequency and voltage in a manner comparable to that of a traditional synchronous machine [3]. Meanwhile, the secondary controller addressed in [4] reinstates the frequency and magnitude deviations generated by the primary controller, which is slower. An in-depth analysis of the similarities that exist between the control of an inverter and that of a synchronous generator in an isolated microgrid can be found in [5]. Sustaining the microgrid frequency and voltage within an appropriate range in distributed generation (DG) in a microgrid presents significant operational and control challenges. In [6], an adaptive control-based dynamic voltage regulation is suggested. The proposed control and battery management system is understudied in the context of Solar PV microgrid V-f and P-Q control literature.

For PV converter Numerous MPPT, control techniques have been examined in the literary work [7,8]. As traditional MPPT approaches, perturb and observe (P&O), hill climbing (HC), and incremental conductance (INC) are examined [9,10]. P&O and HC techniques are easier to implement in hardware, but they include high oscillations that are closer to an MPPT, which causes power losses. The INC approach is precise and adaptable under varying meteorological conditions. However, it has complicated simulation and experimentation. However, with fluctuating sun irradiation, the aforementioned algorithms are ineffective. Artificial neural network (ANN) and intelligent fuzzy logic control (FLC) approaches are thus chosen as MPPT trackers to address the shortcomings of traditional MPPT algorithms under variable weather situations [11]. Fuzzy systems' derived rules and member functions both depend on probability to decide how the system will work. The examination of them is immoderate and sensitive to parameter changes. ANN techniques, on the other hand, depend on learned information and a multi-layered structure. The primary problem with this strategy is that there are no rules for establishing layer architecture. Furthermore, FLC and ANN are both comprehensive approaches to intelligence. An ANFIS technique is a rule base of inference that uses learning data to accelerate the calculations required for factual modeling while retaining high accuracy [12]. The PSO method is used to modify the MPPT and the parameters of PI controller which in turn compensates for the model's unaccounted-for losses and significantly reduces DC-link voltage overshoots [13]. Particle swarm optimization (PSO), firefly algorithm, artificial bee colony (ABC), and ant colony optimization (ACO) are examples of contemporary AI approaches that are utilized to address optimized problems [14,15]. PSO produces an excellent result with little user adjustment. The PSO approach has several benefits over the optimization methods mentioned above, including a lower sample point, simpler mathematical analysis, simple hardware implementation, and cost-effective computer estimate. It also enables quick and accurate PV power monitoring under various operating conditions.

The effectiveness of renewable power systems is currently a top concern related to optimization problems and a burgeoning research area for academia. The industry's specialists cannot discuss the offered optimization problems' intricate mathematical formulations. By combining knowledge from academia with applications in the industrial sector, optimization challenges may be addressed with microgrids, to maintain a voltage regulation goal in addition to frequency controlling.

This research presents a coordinated control algorithm that could be used to enhance PV generation and its ability to control voltage and frequency as well as an active and reactive power in both off-grid and grid-connected microgrids. For this study, precise models of PV systems with two MPPT methods such as P&O and PSO-ANFIS were studied, and the proposed PSO-ANFIS-based control method was developed with photovoltaic functioning and microgrid integration. The most important thing about this work is the novelty of controllers that lie in the coordination in a system among the proposed controllers. These include the control on the PV side with maximum power point tracking (MPPT), battery energy storage system (BESS) control, and V-f and P-Q control in the

inverter. By integrating the proposed PSO_ANFIS MPPT control method which provides fast convergence, zero steady-state error achieving the power balancing aim at either side of the converter can invariably manage the DC side voltage at the right value to keep the AC side voltage at the utility necessary level. This work presents accurate power sharing maintaining stable frequency and voltage in grid-connected mode as well as an autonomous microgrid mode which is a significant contribution to the presented work. In addition, the controls can easily switch from one mode to another, for example, from utility P-Q to V-f controller in isolated operation, without any loss of performance. It has been found that the offered methods of control are effective. The measured values of voltages and current are used to design the controls in abc-dq0 reference frames. As a result, it is simple and quick to build, and also it eliminates the need for transforming between different reference frames, hence making the controller much simpler.

The structure of the paper is as follows: Section 2 depicts the analytical modeling of photovoltaic systems with the proposed PV MPPT control and coordinated P-Q control. Section 3 describes a BESS with the unit of synchronization and droop control method. Section 4 provides compelling evidence that the suggested control strategies are effective. Finally, Section 5 provides a summary of the paper.

2. Photovoltaic Systems with P-Q Control Method

The two inverters and utility test microgrid electrical energy network are shown in Figure 1. The following are the main parts of the proposed microgrid: Solar PV, BESS, and Grid. For this study, MATLAB/SIMULINK is used to simulate a two-inverter, three-phase, grid-based test microgrid. A distribution line of the grid is connected to the PV system and BESS inverters. The PCC is where loads are linked. For one inverter, the input is a PV system followed by a boost converter. For the other inverter, the input is a BESS. In microgrid mode, the two inverters and the grid work together in a coordinated PQ and droop-controlled islanded mode to keep system frequency and bus voltages stable while making sure that generation and load are balanced.
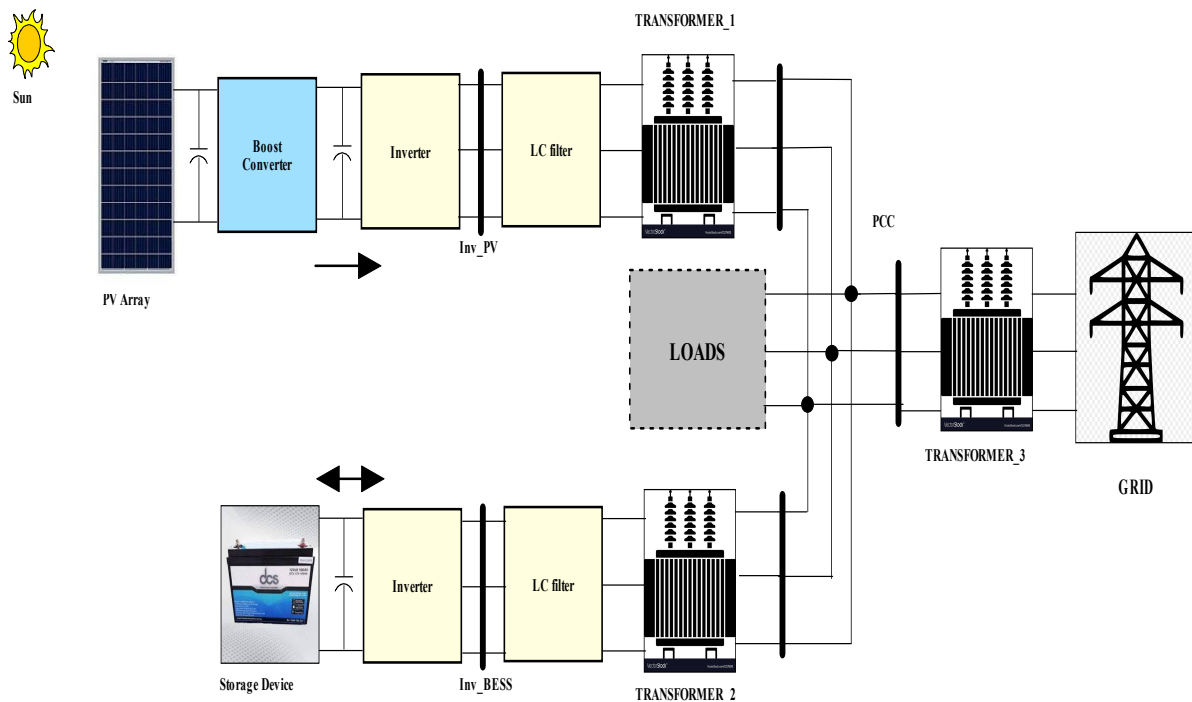

Figure 1. AC microgrid architecture.

2.1. Solar PV Modeling and System Configuration

Figure 2 shows the equivalent circuit for the practical solar cell. The physics of semiconductors gives us the basic equation that describes the I–V characteristic of an ideal solar cell in a mathematical way [16]. It is as follows in (1):

$$I = I_{pv,cell} - \underbrace{I_{o,cell}\left(\exp\left(\frac{qV}{akT}\right) - 1\right)}_{I_d} \tag{1}$$

where I_d is the Shockley diode equation, $I_{o,cell}$ [A] is the reverse saturation or leakage current of the diode [A], $I_{pv,cell}$ is the current produced by incident light (directly proportional to Sun irradiation), a is the diode ideality constant, T [K] is the temperature of the p-n junction, k is the Boltzmann constant, and q is the electron charge $1.602176634 \times 10^{-19}C$.
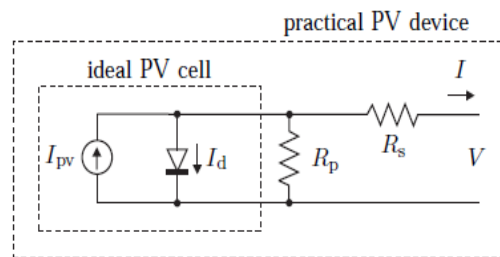

Figure 2. Single-diode model of photovoltaic cell.

The fundamental Equation (1) of the simple photovoltaic cell does not describe the I-V characteristic of an actual solar module. Observation of the features at the solar module terminals demands the addition of extra factors to the fundamental equation because practical modules are composed of several interconnected photovoltaic cells:

$$I = I_{pv} - I_o\left(\exp\left(\frac{V + IR_s}{V_t a}\right) - 1\right) - \frac{(V + IR_s)}{R_p} \tag{2}$$

where I_{pv} and I_o are the photovoltaic and saturation currents of the module, respectively, and $Vt = NskT/q$ is the thermal voltage of the module with Ns cells connected in series. Series-connected cells produce higher output voltages whereas those connected in parallel boost current. The photovoltaic and saturation currents may be stated as $Ipv = Ipv,cellNp$ and $Io = Io,cellNp$, respectively, if the module is made up of parallel connections of cells N_p. In (2), R_p is the equivalent parallel resistance and R_s is the corresponding series resistance of the array. The following equation of array is given as:

$$I_P = N_{Par}I_{pv} - N_{Par}I_o\left(\exp\left(\frac{V + IR_s\left(\frac{N_{Ser}}{N_{Par}}\right)}{V_t a N_{Ser}}\right) - 1\right) - \left(\frac{V + IR_s\left(\frac{N_{Ser}}{N_{Par}}\right)}{R_P\left(\frac{N_{Ser}}{N_{Par}}\right)}\right) \tag{3}$$

where the parameters for each module are I_{pv}, I_o, R_s, R_p, and V_t. Please note that the values of N_s, the series cell numbers within a single solar module, are distinct from N_{ser} in the equation above.

Using the above equations and parameters the adapted photovoltaic modeled with the standard I–V characteristics with MPP under variable irradiance (W/m²) with the cell temperature of 25 °C as shown in Figure 3. The parameters of the PV panel under study are shown in Table 1. The 15 series panels with 190 strings totaling 1 MW are considered under study.
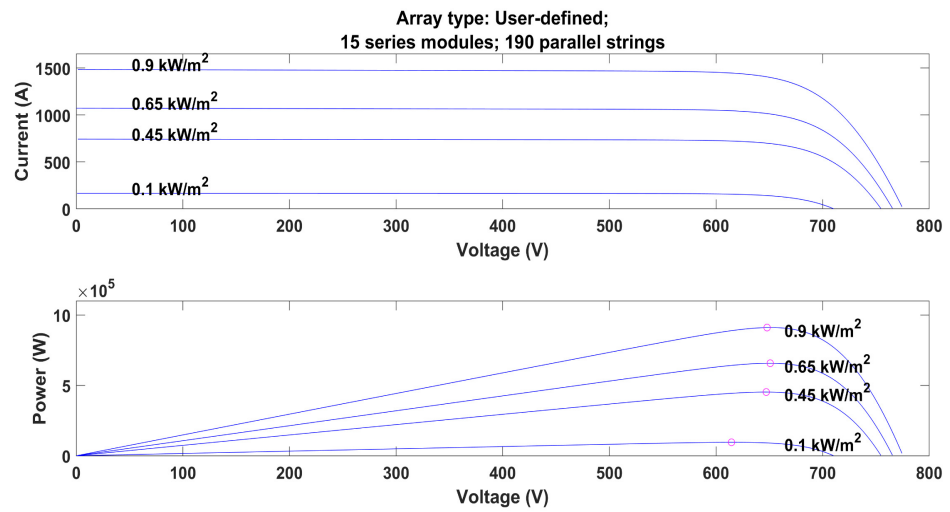
Figure 3. The adopted PV array characteristics.

Table 1. PV panel parameters at 1000 W/m^2 and 25 °C.

Parameters	Nominal Value
P_{MPP}	355.012
V_{MPP}	43.4
I_{MPP}	8.18
V_{OC}	51.9
I_{SC}	8.68

The MPP varies as cell temperature and irradiance change. An MPPT controller controls a converter that is linked to the PV system as shown in Figure 4. The MPPT is affected by both radiation and temperature variation. Thus, under any circumstance, the MPPT controller is guided by the PSO-ANFIS and P&O MPPT algorithms to adjust the operating point in the direction of the MPP [17].
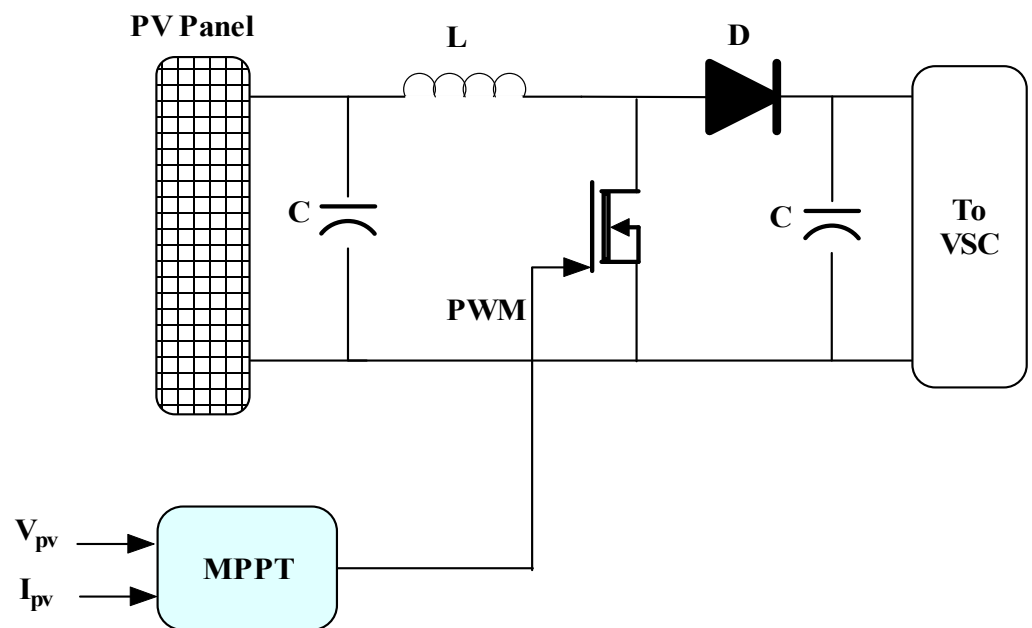

Figure 4. Controller for MPPT boost converter coupled to a PV.

2.2. PSO-ANFIS MPPT Control

The training and refining of ANFIS requirement have become a difficult challenge for developers. The PSO is simpler to implement and has a more rapid convergence rate than gradient algorithms [18]. The PSO also does not require any kind of initial parameter computation or a specific learning rate. The ANFIS controller depicted in Figure 5 is 5 layered as well, a structure of hierarchy whose primary components are antecedents and conclusions. These mathematical formulas describe multilayer feedforward networks:

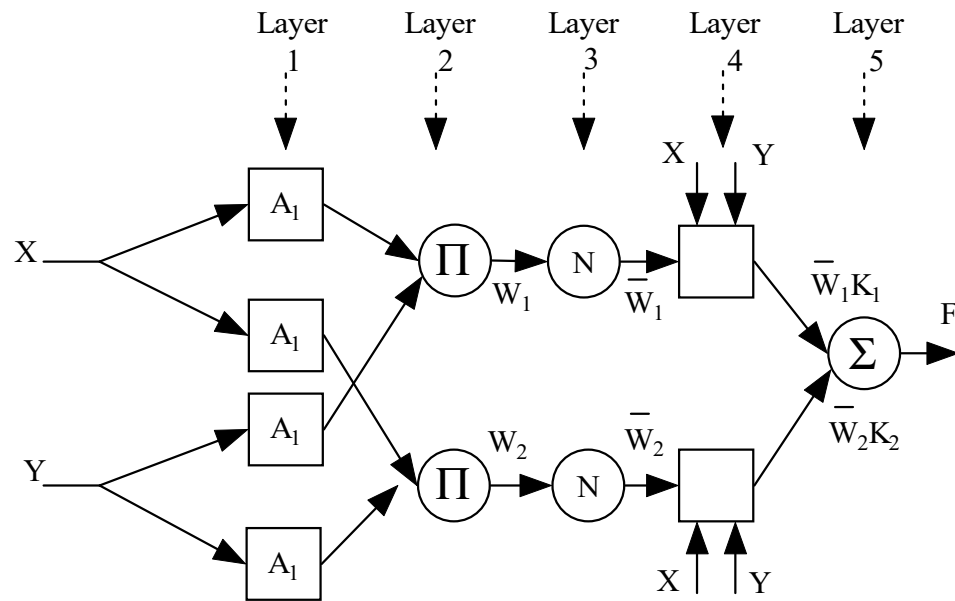$$Wj = \mu p_j(x) * \mu Q_j(y), \; Wj = \frac{W_j}{W_1 + W_2}, \; j = 1, 2. \tag{4}$$

Figure 5. The architecture of an ANFIS controller.

K_1, K_2, and K can be expressed as follows:

$$K_1 = A_1 x + B_1 y + R_1 z, \; K_2 = A_2 x + B_2 y + R_2 z \tag{5}$$

$$K_1 = \frac{W_1 K_1 + W_2 K_2}{W_1 + W_2} = \bar{W}_1 K_1 + \bar{W}_2 K_2 \tag{6}$$

$$\left. \begin{aligned} \mu p_j(x) &= \frac{1}{1 + \left[((x - r_j) p_j)^2 \right]^{bj-3}} \\ \mu p_j(x) &= \exp\left[-\left[\left(\frac{x - r_j}{p_j} \right)^2 \right]^{bj} \right] \end{aligned} \right\} \tag{7}$$

where the parameters p_j, r_j, and b_j are the membership function.

According to the equations given above, the antecedent element can depend on p_j, r_j, and b_j while being trained. Let a_j, b_j, and c_j represent the conclusion components. The number of members of the conclusion component chromosomes is composed as *(N + 1)S*, where *N* is the total amount of data input and *S* is the number of rule bases. Thus, the expression is evaluated by *RMSE* estimations [19,20].

Faster dynamics, a quicker speed of convergence, and a simpler design are just a few benefits this controller provides over conventional MPPT controllers. Fuzzification, inference, and defuzzification processes make up the main building blocks of this approach. Given an input parameter (PV voltage), the final signal of the pulse-width modulation (PWM) created by the MATLAB/Simulink model of a PSO-ANFIS technique is called the

duty ratio. Figure 6 depicts the comprehensive flowchart arrangement of the PSO-ANFIS-based MPPT control. It is necessary to correctly modify the membership values based on the fuzzy data gathered utilizing a potent ANFIS algorithm with learnt training rules before the error is decreased to an absolute minimum. The trained system can function as a controller as MPPT once the appropriate membership parameters have been adjusted.
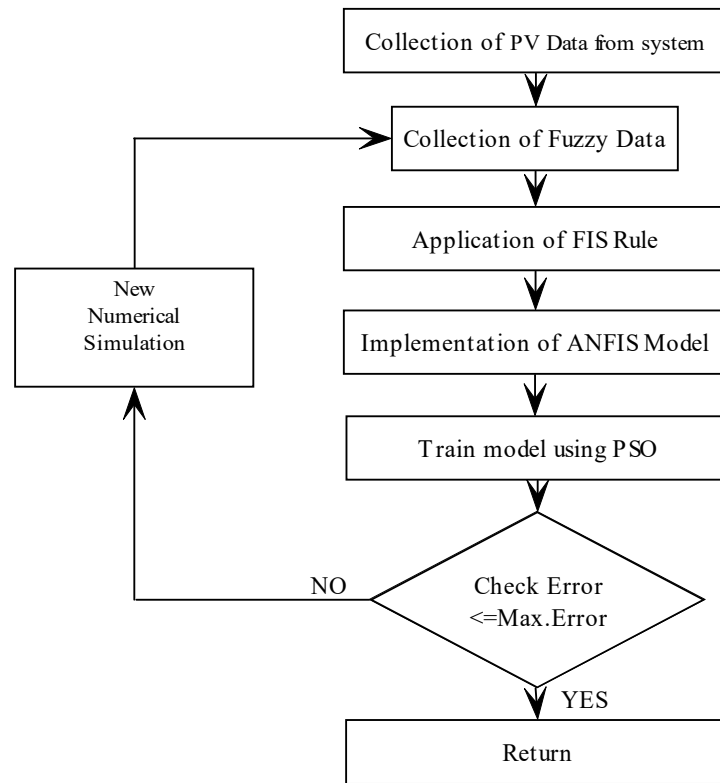

Figure 6. Flowchart of PSO_ANFIS-based MPPT.

This procedure is used to adapt the boost converter duty ratio determined by the flowchart in Figure 6 and the PSO-ANFIS parameters are listed in Table 2 for use during defuzzification.

Table 2. PSO-ANFIS parameters.

Parameters	Nominal Value
No. of operation	25
No. of iteration	100
Weight of inertia	1

The factors of the antecedent/consequent parameters are often examined separately in the conventional method. In this PSO-ANFIS approach, the mean square error is reduced by all parameters being trained and tested simultaneously. The ANFIS architecture's adaptive learning is calculated through online learning evaluation using the input/output parameters. Figures 7 and 8 show the trained and tested data with the error of the PSO-ANFIS controller.
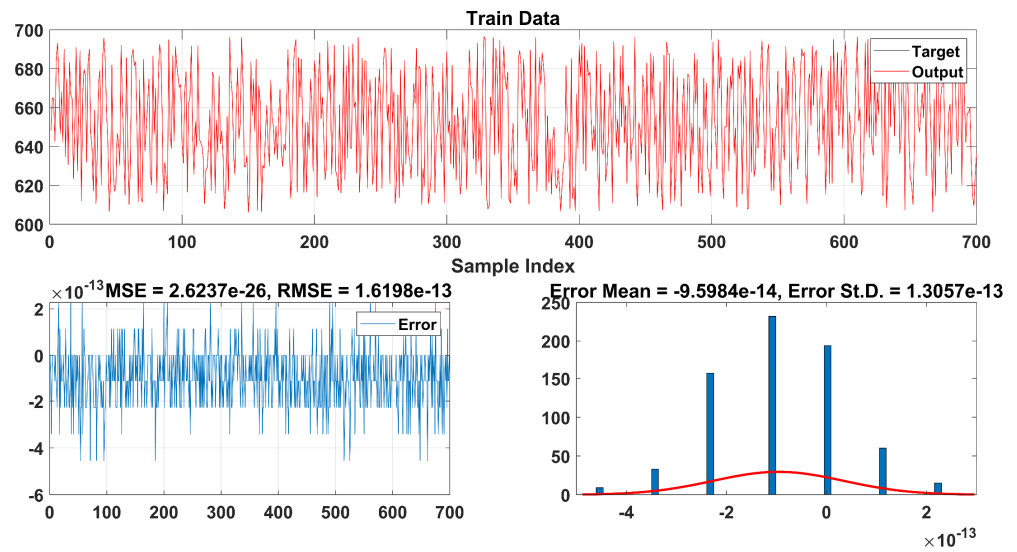
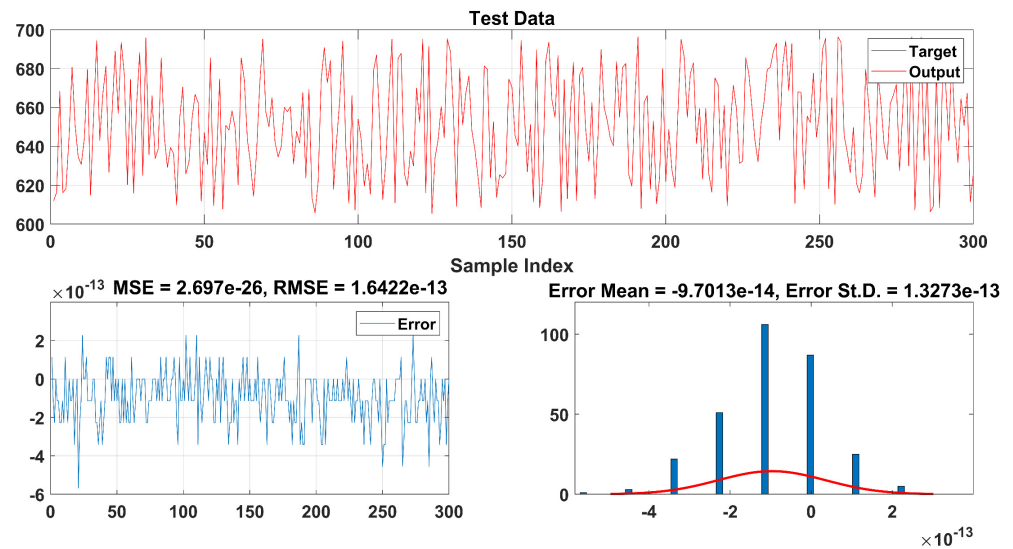**Figure 7.** Train Data with the error of PSO_ANFIS.

Figure 8. Test Data with the error of PSO_ANFIS.

2.3. Inverter Control

The output voltage (DC bus voltage) of the boost converters is maintained at a stable acceptable value. This is given to the inverter to get a three-phase supply to balance the generation and the load using the inverter PQ controller. The DC voltage must constantly remain at an acceptable value for the inverter to control [21], and this is irrespective of how much ever real power the PV system provides. The connection between the inverter and the microgrid is made using an LC power filter on the AC side and a three-phase coupling transformer as shown in Figure 1. The following is the mathematical modeling that is required for a typical three-phase inverter model for a PV system grid-connected as follows.

$$\left. \begin{array}{l} v_a = R_f i_a + L_f \frac{di_a}{dt} + v_{ga} \\ v_b = R_f i_b + L_f \frac{di_b}{dt} + v_{gb} \\ v_c = R_f i_c + L_f \frac{di_c}{dt} + v_{gc} \end{array} \right\} \tag{8}$$

where i_a, i_b, and i_c are the inverter output currents, v_a, v_b, and v_c are the inverter side voltages, v_{ga}, v_{gb}, and v_{gc} are the grid side voltages, and R_f and L_f are the LC power filter resistor and inductor. An equation can be expressed as:

$$\left.\begin{array}{l} \frac{di_a}{dt} = -\frac{R_f}{L_f}i_a - \frac{v_{ga}}{L_f} + \frac{v_a}{L_f} \\ \frac{di_b}{dt} = -\frac{R_f}{L_f}i_b - \frac{v_{gb}}{L_f} + \frac{v_b}{L_f} \\ \frac{di_c}{dt} = -\frac{R_f}{L_f}i_c - \frac{v_{gc}}{L_f} + \frac{v_c}{L_f} \end{array}\right\} \quad (9)$$

The primary responsibilities of the inverter controller are to regulate the DC-link voltage and also to transmit the DG's active power into the grid through the converters. The projected control technique is shown in Figure 9. The voltage loop is fed by the measured DC-link voltage and the reference voltage, to get the reference current. This reference current and the measured current are given to the current control loop to get the reference voltage, which is given to the pulse generator to get the pulses for inverter switches.
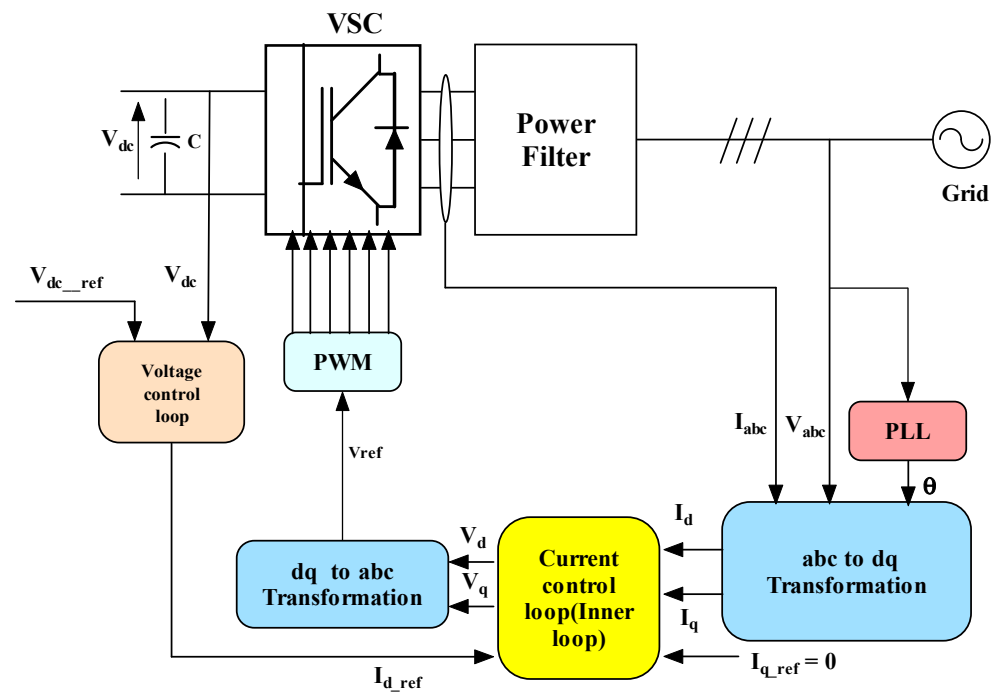

Figure 9. Controller block of three-phase PV inverter.

The transformation is used to generate the reference signal for modulating three-phase inverters from the static reference frame to rotating reference frame park components (dq) as:

$$\begin{bmatrix} d \\ q \end{bmatrix} = \begin{bmatrix} \cos\theta & \sin\theta \\ -\sin\theta & \cos\theta \end{bmatrix} \begin{bmatrix} \alpha \\ \beta \end{bmatrix} \quad (10)$$

The PI regulators of voltage and the current controllers are given as:

$$\left.\begin{array}{l} I_{d-ref} = (k_{pvpv} + \frac{k_{iviv}}{s})(V_{dc-ref} - v_{dc}) \\ I_{q\_ref} = 0 \end{array}\right\} \quad (11)$$

$$\left.\begin{array}{l} V_d = (k_{pib} + \frac{k_{iib}}{s})(I_{dref} - I_d) \\ +V_d - \omega L_{ff}I_{qref} \\ V_q = (k_{pib} + \frac{k_{iib}}{s})(I_{qref} - I_q) \\ +V_q + \omega L_{ff}I_{dref} \end{array}\right\} \quad (12)$$

where k_{pvpv} and k_{ivpv} are the gains of the PV voltage loop PI controller, and the current controller PI gains are k_{pipv} and k_{iipv}.

The suggested method ensures power balance at the DC-link via a precise model of the system, where in the power that needs to be pumped onto the grid is determined precisely using the PSO-ANFIS MPPT method and from the system's observed value. Since the obtained power from the PV source is delivered into the microgrid, thus the current generation is predicted using PI controller with the aim that the DC-link voltage will stabilize. Additionally, the DC-link voltage stability is substantially improved.

3. Battery Energy Storage System (BESS)

The BESS consists of a storage element, which is taken from the MATLAB 2022b version of the SimPowerSystem/Simscape electrical library. As given in the paper about the battery model the deep cycle battery being necessary due to the uncertain weather, the parameters are appropriately used as needed for the controller [22]. The equation of discharge and charge Lithium-ion Iron Phosphate (LFP) battery model is given as [23],

$$V_{BAT} = V_0 - R.i - K\frac{Q}{(Q - \text{it})}(\text{it} + \text{t}^*) + A.\exp(-B.\text{it}) \tag{13}$$

$$V_{BAT} = V_0 - R.i - K\frac{Q}{(\text{it} - 0.1Q)}i^* - K\frac{Q}{(Q - \text{it})}.\text{it} + A\exp(-B.\text{it}) \tag{14}$$

where V_{BAT} is the battery voltage (V), V_0 is the battery constant voltage (V), K is polarization constant (V/Ah), Q is battery capacity (Ah), it is the actual battery charge (Ah), R is the internal resistance (Ω), i is battery current (A), i^* is filtered current (A), A is exponential zone amplitude (V), and B is exponential zone time constant inverse (Ah).

The solar power output varies, and load variability is the reason to use a storage system for the microgrid application. The battery system has 1 MWh of backup energy to balance PV power for the critical load and frequency control. The other elements in this system are an inverter, filter, and coupling transformer. Figure 10 shows the BESS controller, which generates a reference voltage to the PWM block. The controller consists of droop control, a power and voltage regulator, and current controller. To ensure the system frequency and voltage while ensuring the generation load balance. The control methodology is explained below.
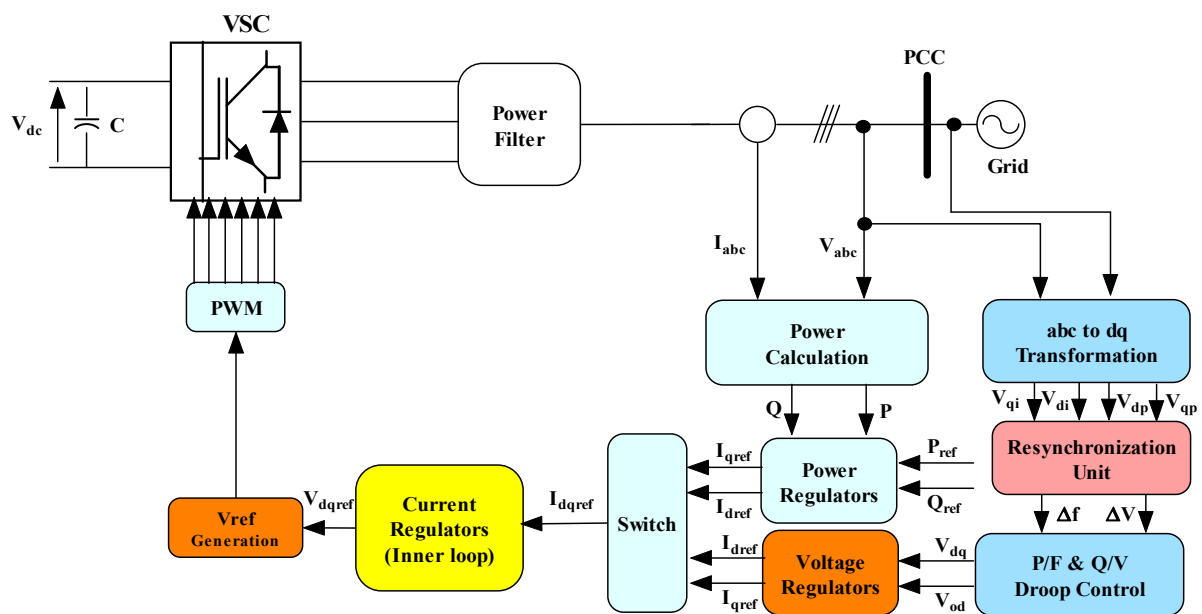

Figure 10. The storage system inverter controller.

3.1. Unit of Resynchronization

The microgrid out-of-phase recloses with the supply system, leading to incredibly high inrush currents. Instead, the microgrid voltage is in phase with the distribution voltage; the resynchronization system will prevent a blackout. Operating this will ensure a soft reconnection to the supply system. Three seconds will pass during the synchronization process. The voltage and frequency will gradually catch up to that of the central grid using PI regulators.

The voltage and frequency deviations computed using PLL are computed using the resynchronization block as in [24,25]. The primary droop will be modified to include these deviations to account for the altered voltage or frequency. The instantaneous complex powers of the inverter in dq reference frame and the power on the DC side P_{dc} of the inverter are represented as:

$$P_{dc} = V_{dc}I_{dc} \tag{15}$$

$$\left.\begin{array}{l} P = \frac{3}{2}(V_d I_d + V_q I_q) \\ Q = \frac{3}{2}(V_d I_d - V_q I_q) \end{array}\right\} \tag{16}$$

3.2. Droop Controller

In the microgrid under the grid-forming mode, the BESS must control the microgrid's voltage and frequency. The BESS has a droop P/F put to 0.5%, (the inverter produces its nominal active power). The microgrid voltage at the PCC bus can be adjusted by the adjustment of the droop Q/V put to 3%. Hence, droop control serves two purposes: it regulates real/reactive power using frequency/voltage control [26,27]. The following is how a droop control equation is created. A transmission line's actual and reactive power are as follows:

$$\left.\begin{array}{l} P = \frac{V_1 V_2}{X} \sin \delta \\ Q = -\frac{V_1 V_2}{X} \cos \delta + \frac{V_1^2}{X} \end{array}\right\} \tag{17}$$

The power angle (δ) is much lower, so Sin δ = δ and Cos C = 1. Hence, equations become

$$\delta = \frac{PX}{V_1 V_2} \tag{18}$$

$$V_2 - V_1 \cong -\frac{XQ}{V_1} \tag{19}$$

The preceding equations demonstrate that power angle control can be done using real power. The voltage can be managed using reactive power. Frequency control results in power angle regulation, which controls the actual power flow [28]. So, the frequency and voltage droop control can be calculated as follows:

$$\left.\begin{array}{l} f = f_s + k_{pf}(P - P^s) \\ V = V_s + k_{QV}(Q - Q^s) \end{array}\right\} \tag{20}$$

The measured and set values of frequency, voltage, and active and reactive power are denoted as f, V, P, and Q, and f_s, V_s, P_s, and Q_s, respectively. Droop proportional constants are k_{pf} and k_{QV}.

3.3. Power and Voltage Regulators

In the microgrid mode, the voltage regulator is set and computes I_d and I_q from the measured dq voltages and the voltage reference V_{ref} which is generated by the droop controller. Under the grid mode, the active and reactive power regulators are set. The power regulators are used to produce I_{dref} and I_{qref} reference currents using the measured

and reference active/reactive power. The voltage regulator and power regulator governing equation with PI controller are given in (21 and 22) as [29,30] as shown in Figure 10.

$$\left. \begin{aligned} I_d &= (k_{pvb} + \tfrac{k_{ivb}}{s})(V_{ref} - V_d) \\ I_q &= (k_{pvb} + \tfrac{k_{ivb}}{s})(0 - V_q) \end{aligned} \right\} \tag{21}$$

$$\left. \begin{aligned} I_{dref} &= (k_{ppb} + \tfrac{k_{ipb}}{s})(P - P_{ref}) \\ I_{qref} &= (k_{pqb} + \tfrac{k_{iqb}}{s})(Q - Q_{ref}) \end{aligned} \right\} \tag{22}$$

where k_{pvb} k_{ivb} and k_{ppqb}, k_{ipqb} are the PI gains of the BESS voltage controller and the power controller, respectively.

3.4. Current Regulators

The processed currents which are obtained from the voltage regulator (isolated) mode or power regulator (grid mode) through switch are fed to the Current Regulator. To produce the required dq voltages to generate pulses for the inverter, it is important to note that the regulators use feedforward computation to achieve a high dynamical response. Current control functions as an inner loop section on the control of inverters. The PI controllers control keeps track of current reference values, respectively. The PI controller output, the dq voltage, and the cross voltage drop in the resistor and inductor R_{ff} and L_{ff} are combined to generate the reference voltages V_{drref} and V_{qrref}. This reference voltage is used to generate the PWM, which creates the necessary commands for the switches on the grid-connected inverter [31–33]. The equation is given as:

$$\left. \begin{aligned} V_{dref} &= (k_{pib} + \tfrac{k_{iib}}{s})(I_{dref} - I_d) \\ &+ V_d - \omega L_{ff} I_q \\ V_{qref} &= (k_{pib} + \tfrac{k_{iib}}{s})(I_{qref} - I_q) \\ &+ V_q - \omega L_{ff} I_q \end{aligned} \right\} \tag{23}$$

where k_{pib} and k_{iib} are the PI values for the BESS current loop controller. The translated and scaled V_{dref} and V_{qref} are used to generate a three-phase reference signal V_{ref}, and then fed to the PWM block to produce pulses for the inverter switches.

4. Results and Discussion

The simulation results for the test microgrid with the proposed P-Q and droop control method are presented in this section with PSO-ANFIS MPPT control. First, the grid-connected mode with the coordinated P-Q control method is considered. After that, droop control coordination is shown, with a BESS and a PV system coupled to PCC in an island scenario.

4.1. Grid Connected Mode

The study on PQ controllers with integrated MPPT such as PSO-ANFIS with battery control is summarized here. Tables 3 and 4 show the controller gain parameters. The proposed PSO-ANFIS MPPT method has an edge in terms of precise and rapid power (PPV) as shown in Figure 11, i.e., from 0.1 s to 0.2 s. Additionally, from 4.4 s to 4.5 s, the settling the power to steady state is faster than P&O method. The demand for active power is met with PV power, storage system, and the grid. The coordinated P-Q control is tested, and the result shown here determines the effectiveness of the suggested control.

Table 3. Photovoltaic System Data.

Symbol	Description	Nominal Value
K_{ppv}	Power regulator Proportional gain	0.05
K_{ipv}	Power regulator Integral gain	2
K_{pvpv}	Current regulator Proportional gain	6
K_{ivpv}	Current regulator Integral gain	30
K_{pipv}	Voltage regulator Proportional gain	0.2
K_{iipv}	Voltage regulator Integral gain	15
F_{sw}	PWM switching freq. Hz	2700
K_{psvn}	Sync. Proportional gain (Kpsyn)	0.075
$Kisvn$	Sync. Integral gain	0.03

Table 4. Battery Energy Storage System Data.

Symbol	Description	Nominal Value
K_{pf}	Frequency droop	0.5
K_{QV}	Voltage droop	3
K_{ppb}	Power regulator Proportional gain	1.5
K_{ipb}	Power regulator Integral gain	15
K_{pib}	Current regulator Proportional gain	0.2
K_{iib}	Current regulator Integral gain	15
K_{pvb}	Voltage regulator Proportional gain	2
K_{ivb}	Voltage regulator Integral gain	25
F_{sw}	PWM switching freq. Hz	2700
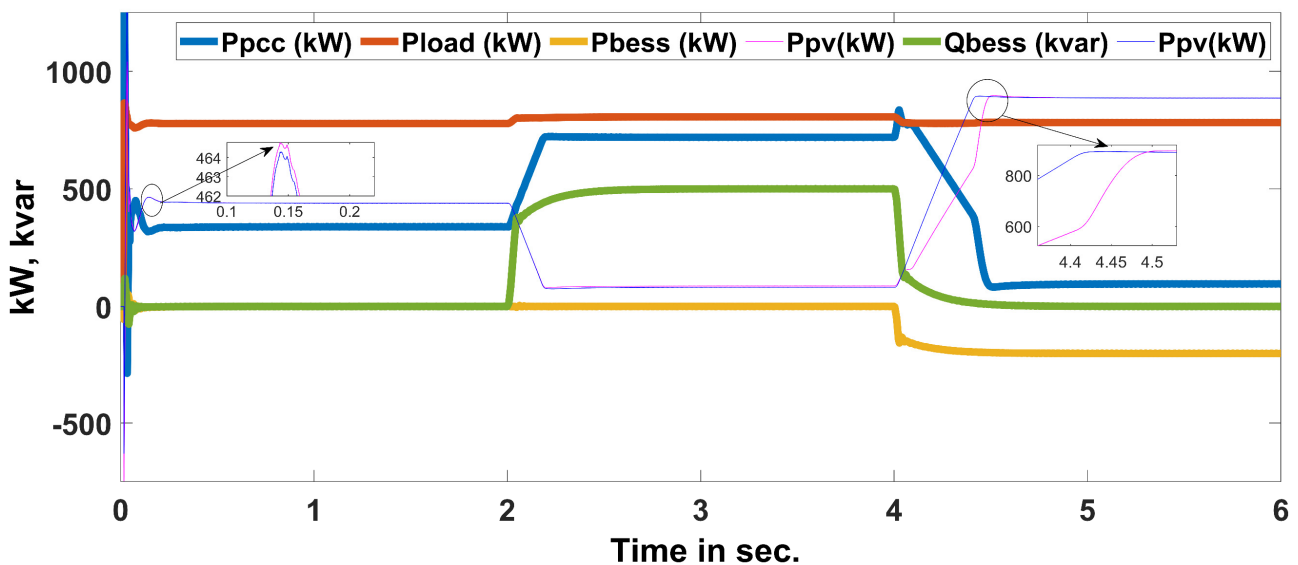
Figure 11. Power sharing of the system.

Figure 11 shows the active power requirement by the load met by the grid and the solar PV system. The excess generation by PV will be stored in the battery storage device.

The load terminal voltage Vrms as shown in Figure 12, as the voltage stays almost constant at about 415 V irrespective of load variation. The solar PV system with PSO-ANFIS controller tracks MPP as it is shown in Figure 4 in accordance with irradiance as depicted in Figure 13; the PV system produces power accordingly during the simulation's time frame.
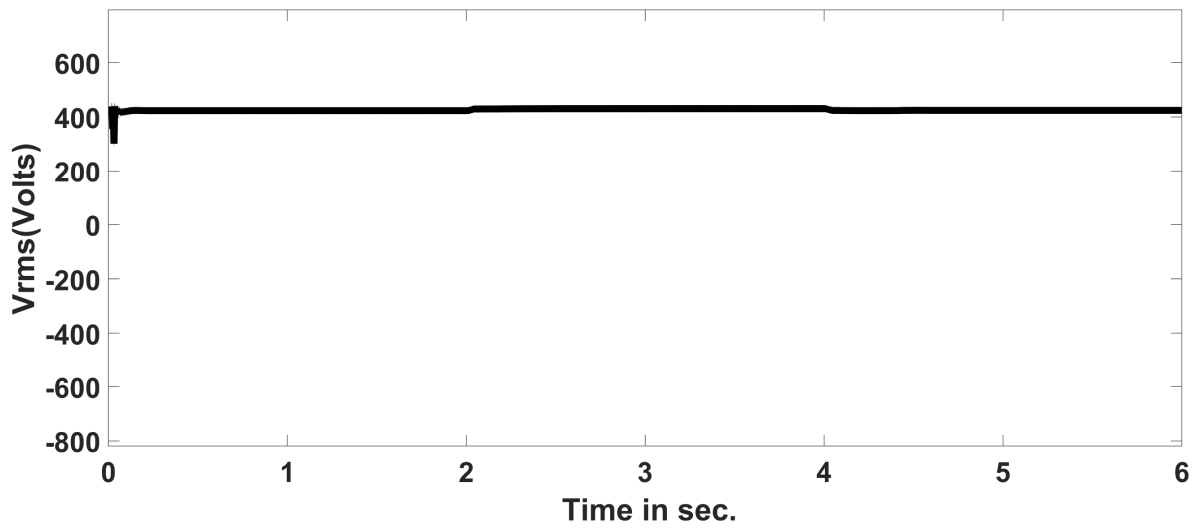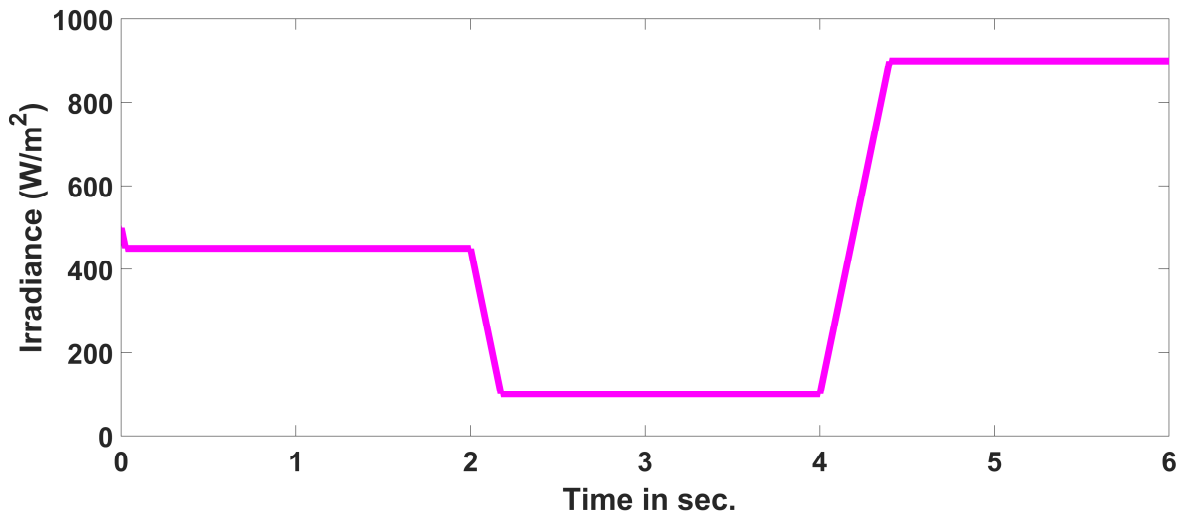
Figure 12. PCC Voltage.

Figure 13. Solar irradiation.

Considering the solar irradiation is about 900 W/m2 at 4 s as shown in Figure 13, the PV system produces power of almost 1 MW, which is more than enough to sustain the frequency of the microgrid. Thus, the controller act such that the battery gets charged with excess power. The battery power shows a negative sign in the charging mode, indicating that the battery is absorbing energy. These references illustrate both the discharging and charging phases of the standby energy storage battery positive and negative, respectively. As irradiance varies, PV effectively operates at MPP. When PV system energy is not enough to hold up the frequency of the microgrid at an acceptable value of almost 50 Hz, the grid provides a deficit power as shown in Figure 11. Figures 14 and 15 show the boost converters regulating voltage of the PV system and storage device, respectively, choosing initially the battery state of charge (SoC) at 50%. As demand is constant, the PV system generates excess power due to an increase in irradiance at 4 s when the battery starts charging; i.e., the SoC slope becomes positive as shown in Figure 16. The battery keeps charging and discharging for 6 h, which is investigated with 6 s.
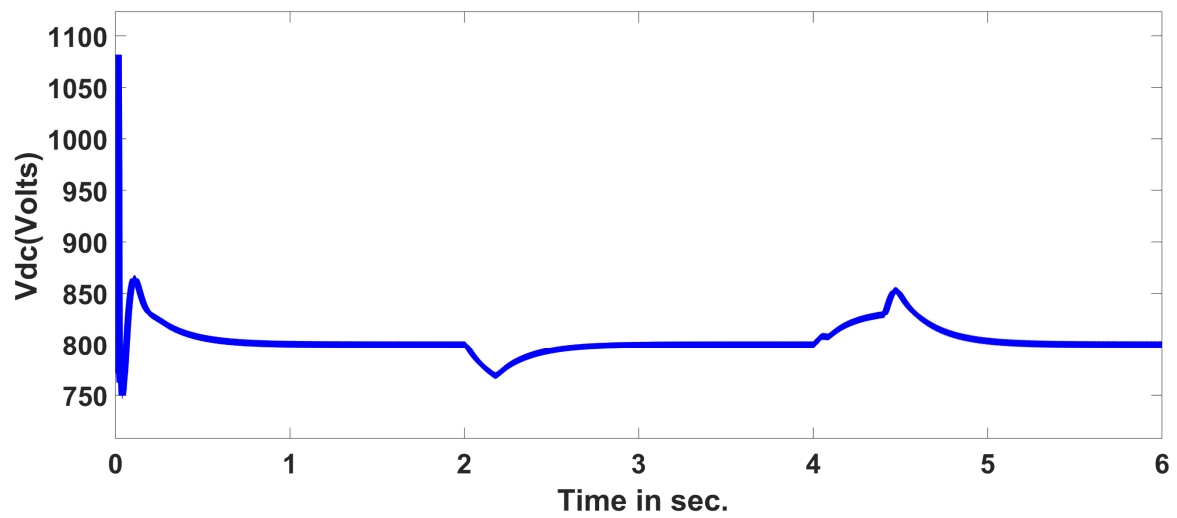
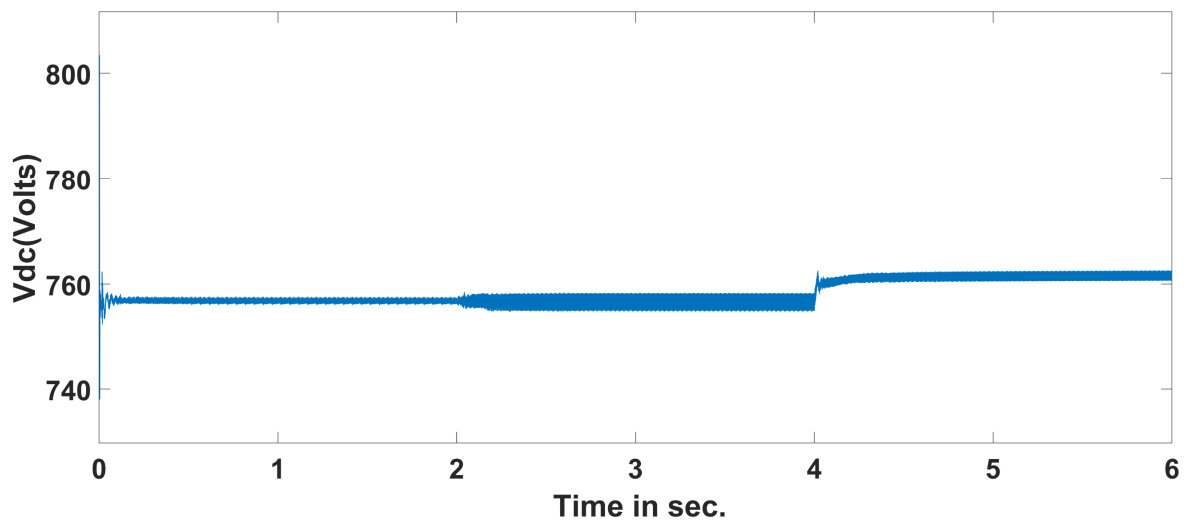**Figure 14.** Output voltage of boost converter.

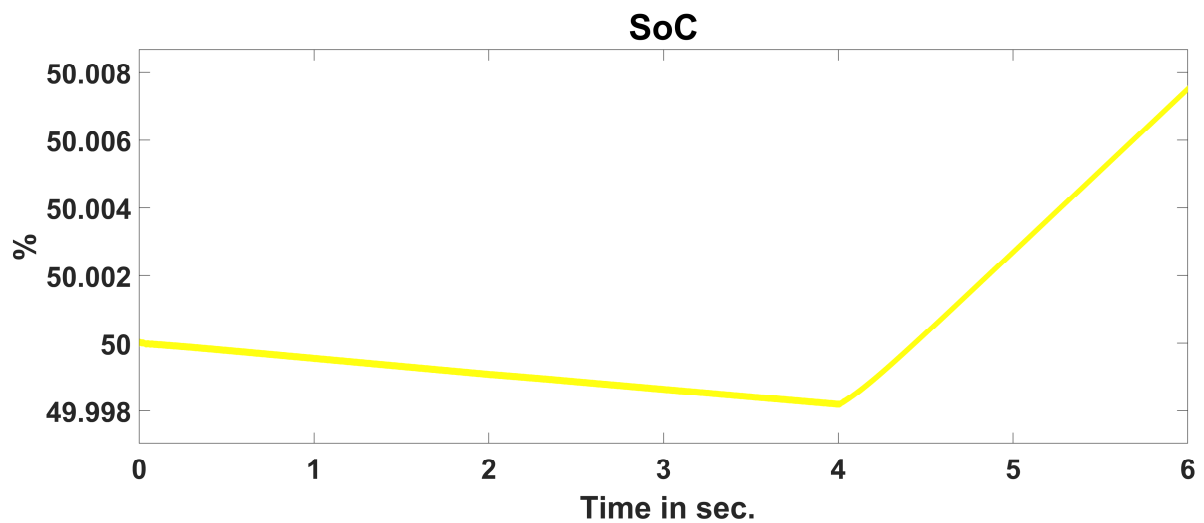**Figure 15.** Battery energy storage system charging voltage.

Figure 16. Battery energy storage SoC.

Hence, the constant DC link voltage is provided to the inverter. This is processed from the PSO_ANFIS method to get the duty ratio for the boost converter to extract the maximum power from the PV system. Along with the proper controller, the DC-link voltage stability is maintained as shown in Figure 14. Hence, the power balance indicates that the coordinated P-Q proposed controller is appropriate in microgrids.

4.2. Grid to Microgrid to Grid Mode

An additional case study demonstrates the dynamic features of the suggested control algorithms during grid-to-microgrid and back-to-grid transitions. In this study, the system first acts as a standard grid, and then the tie switch is opened after one second to make an intentional island. As a result, the microgrid is solely reliant on the PCC's solar farm and BESS. The combined real and reactive power infusion from the BESS inverter and solar plant with PSO-ANFIS during microgrid mode is shown in Figure 17. The controller instructs the solar plant to produce an assuring of active power at MPP when it switches from grid-connected to microgrid mode based on the irradiance which is constant in this case; the irradiance is at $650\,\text{W/m}^2$, so the solar plant produces a consistent 650 kW throughout the study. In a microgrid-connected mode, i.e., when it transits to the islanded condition, the PV system is managed to provide real power, and the deficit power required for the load is covered by the BESS inverter system with reactive power. As the microgrid transitions to the islanded situation, there are both active and reactive power injections from the PV system and battery.
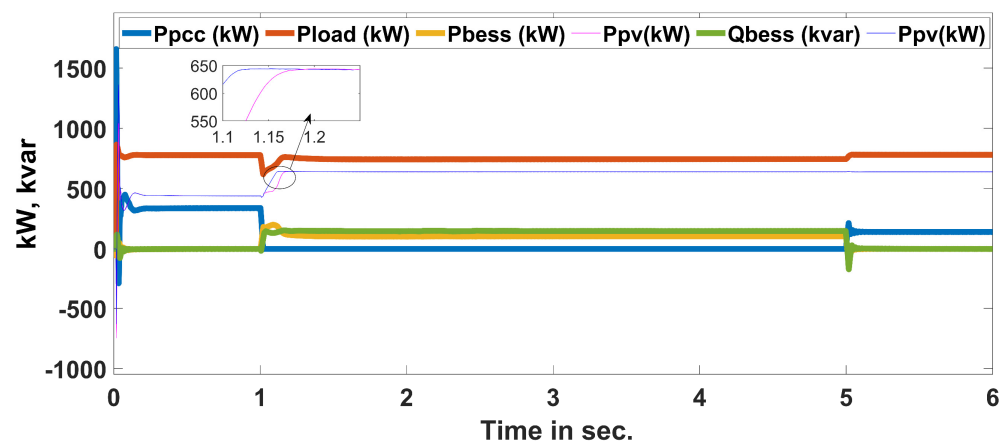

Figure 17. Power sharing of the system.

Inverters are in charge of keeping the microgrid frequency and voltage at the PCC level. In the isolated mode, the solar plant's active power is insufficient to supply the microgrid's energy demands due to irradiance of $650\,\text{W/m}^2$. The microgrid frequency drops to 49.9 Hz because of the mismatch in load and generation. The controller from the BESS begins within seconds and immediately returns to the normal value as shown in Figure 18. Additionally, the PCC voltage of almost acceptable value of 415 V in rms even though considering step load variation by injecting reactive power during 1 to 5 s is shown in Figure 19. Following the start of the control, the voltage is swiftly regulated at 415 Vrms. Figures 20 and 21 show the boost converters regulated voltage with PSO-ANFIS MPPT for the PV system and storage device, respectively. Similarly, under microgrid mode, choosing initially the battery State of charge (SoC) is at 50%. It was discharging as demand was more between 1 to 5 s as grid power was intentionally made unavailable solely on microgrid mode, so the SoC slope becomes negative up to 5 s as shown in Figure 22. The battery keeps charging and discharging for 6 h, which is investigated for 6 s. At 5 s, when the grid is again made available, the slope becomes zero. Thus, the results shown here make clear that the droop and inverter control along with the PSO-ANFIS MPPT for PV converter operates effectively under grid-isolated-grid mode.
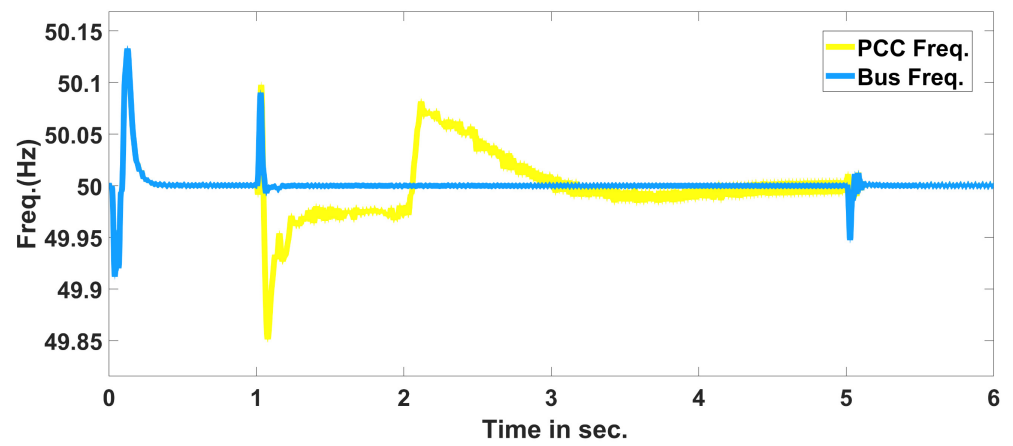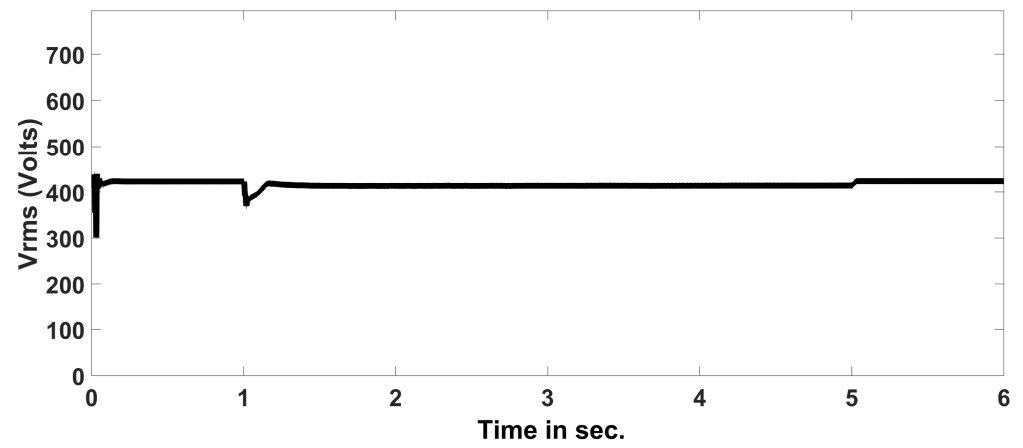
Figure 18. Frequencies of microgrid and PCC.
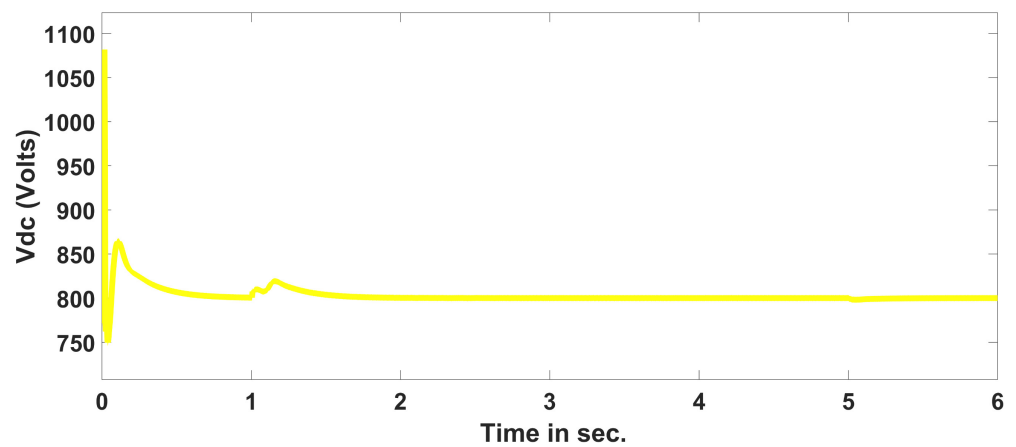

Figure 19. PCC Voltage.

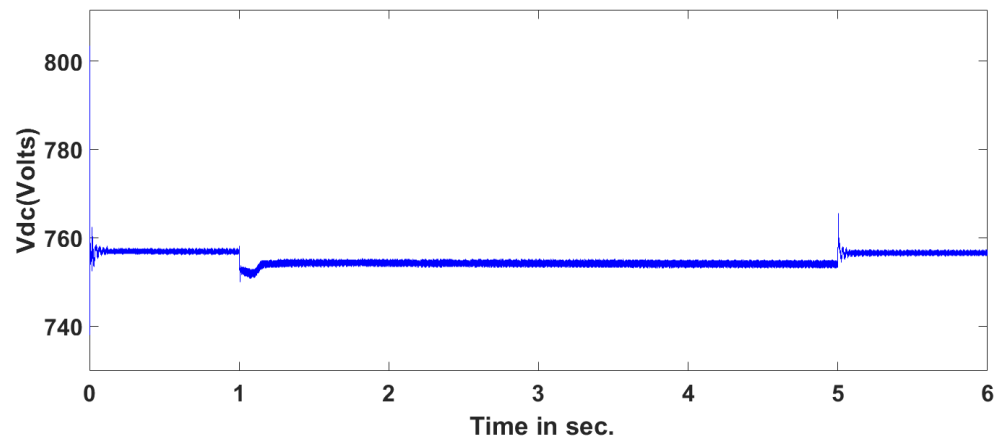**Figure 20.** Output voltage of PV boost converter.

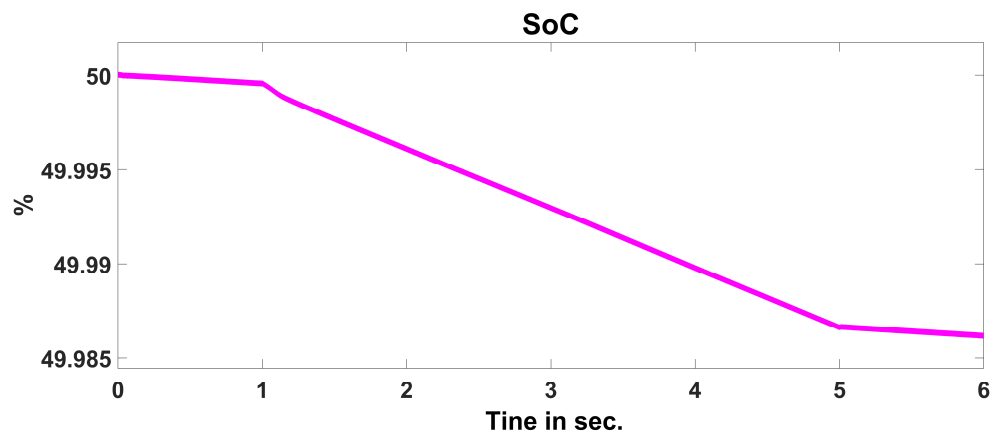**Figure 21.** Energy storage Voltage.

Figure 22. Battery energy storage SoC.

The suggested ANFIS-PSO algorithm effectively and quickly monitors MPP in all patterns in the grid and islanded mode. In comparison to the traditional P&O-based MPPT approach, the proposed PSO-ANFIS-based MPPT has a swift convergence velocity, high PV monitoring efficiency due to the least RMSE, and the ability to produce a quick MPP region.

5. Conclusions

The proposed work demonstrates coordinated V-f/P-Q techniques for the grid and islanded mode using a photovoltaic system with PSO-ANFIS MPPT and battery storage. In this work, the photovoltaic system is run with two methods to obtain maximum power point (MPP). The proposed PSO-ANFIS MPPT method has an edge over the P&O method for quick, accurate, and exact PV tracking in variable irradiance. Along with the proposed control method, a seamless change from grid-connected side PQ control to island V-f management back to grid resynchronization, respectively, was seamless and successful. In the suggested microgrid, the V-f control mechanism brings back the microgrid frequency and PCC voltage with the use of battery installations. The battery storage acts as a buffer to inject and receive power as needed via the charge/discharge cycle to make up for any shortfalls or surpluses. Additionally, the coordinated PQ control method under the grid follows the mode of the active power requirement by the load met by the grid, the solar PV system, and the storage device. The excess generation by PV will be stored in the battery storage device. The limitation is, the larger the data, the convergent time is large with the proposed method. The proposed work can be extended with the Internet of Things-based MPPT control method, also for partial shading of photovoltaic as the future scope.

References

1. Vandoorn, T.L.; Vasquez, J.C.; De Kooning, J.; Guerrero, J.M.; Vandevelde, L. Microgrids: Hierarchical control and an overview of the control and reserve management strategies. *IEEE Ind. Electron. Mag.* **2013**, *7*, 42–55. [CrossRef]
2. Chowdhury, S.; Chowdhury, S.P.; Crossley, P. *Microgrids and Active Distribution Networks*; Instutation of Engineering and Technology: London, UK, 2022. [CrossRef]
3. Kim, J.S.; So, S.M.; Kim, J.T.; Cho, J.W.; Park, H.J.; Jufri, F.H.; Jung, J. Microgrids platform: A design and implementation of a common platform for seamless microgrids operation. *Electr. Power Syst. Res.* **2019**, *167*, 21–38. [CrossRef]
4. Vasquez, J.C.; Guerrero, J.M.; Savaghebi, M.; Eloy-Garcia, J.; Teodorescu, R. Modeling, analysis, and design of stationary-reference-frame droop-controlled parallel three-phase voltage source inverters. *IEEE Trans. Ind. Electron.* **2012**, *60*, 1271–1280. [CrossRef]
5. Vandoorn, T.L.; Meersman, B.; De Kooning, J.D.; Vandevelde, L. Analogy between conventional grid control and islanded microgrid control based on a global DC-link voltage droop. *IEEE Trans. Power Deliv.* **2012**, *27*, 1405–1414. [CrossRef]
6. Li, H.; Li, F.; Xu, Y.; Rizy, D.T.; Adhikari, S. Autonomous and adaptive voltage control using multiple distributed energy resources. *IEEE Trans. Power Syst.* **2012**, *28*, 718–730. [CrossRef]
7. Zadeh, M.J.Z.; Fathi, S.H. A new approach for photovoltaic arrays modeling and maximum power point estimation in real operating conditions. *IEEE Trans. Ind. Electron.* **2017**, *64*, 9334–9343. [CrossRef]
8. El Aamri, F.; Maker, H.; Sera, D.; Spataru, S.V.; Guerrero, J.M.; Mouhsen, A. A direct maximum power point tracking method for single-phase grid-connected PV inverters. *IEEE Trans. Power Electron.* **2017**, *33*, 8961–8971. [CrossRef]
9. Khan, O.; Acharya, S.; Al Hosani, M.; El Moursi, M.S. Hill climbing power flow algorithm for hybrid DC/AC microgrids. *IEEE Trans. Power Electron.* **2017**, *33*, 5532–5537. [CrossRef]
10. Huynh, D.C.; Dunnigan, M.W. Development and comparison of an improved incremental conductance algorithm for tracking the MPP of a solar PV panel. *IEEE Trans. Sustain. Energy* **2016**, *7*, 1421–1429. [CrossRef]
11. Al-Gizi, A.G.; Craciunescu, A.; Al-Chlaihawi, S.J. The use of ANN to supervise the PV MPPT based on FLC. In Proceedings of the 2017 10th International Symposium on Advanced Topics in Electrical Engineering (ATEE), Bucharest, Romania, 23–25 March 2017; IEEE: Piscataway, NJ, USA, 2017; pp. 703–708.
12. Mir, M.; Kamyab, M.; Lariche, M.J.; Bemani, A.; Baghban, A. Applying ANFIS-PSO algorithm as a novel accurate approach for prediction of gas density. *Pet. Sci. Technol.* **2018**, *36*, 820–826. [CrossRef]
13. Ahmed, M.; Abdelrahem, M.; Farhan, A.; Harbi, I.; Kennel, R. DC-link sensorless control strategy for grid-connected PV systems. *Electr. Eng.* **2021**, *103*, 2345–2355. [CrossRef]
14. Sundareswaran, K.; Vigneshkumar, V.; Sankar, P.; Simon, S.P.; Nayak, P.S.R.; Palani, S. Development of an improved P&O algorithm assisted through a colony of foraging ants for MPPT in PV system. *IEEE Trans. Ind. Inform.* **2015**, *12*, 187–200.
15. Lee, J.; Kim, Y. Comparative Estimation of Electrical Characteristics of a Photovoltaic Module Using Regression and Artificial Neural Network Models. *Electronics* **2022**, *11*, 4228. [CrossRef]
16. Villalva, M.G.; Gazoli, J.R.; Ruppert Filho, E. Modeling and circuit-based simulation of photovoltaic arrays. In Proceedings of the 2009 Brazilian Power Electronics Conference, Bonito-Mato Grosso do Sul, Brazil, 27 September–1 October2009; IEEE: Piscataway, NJ, USA, 2009; pp. 1244–1254.
17. Islam, H.; Mekhilef, S.; Shah NB, M.; Soon, T.K.; Seyedmahmousian, M.; Horan, B.; Stojcevski, A. Performance evaluation of maximum power point tracking approaches and photovoltaic systems. *Energies* **2018**, *11*, 365. [CrossRef]
18. Priyadarshi, N.; Padmanaban, S.; Holm-Nielsen, J.B.; Blaabjerg, F.; Bhaskar, M.S. An experimental estimation of hybrid ANFIS–PSO-based MPPT for PV grid integration under fluctuating sun irradiance. *IEEE Syst. J.* **2019**, *14*, 1218–1229. [CrossRef]
19. Priyadarshi, N.; Padmanaban, S.; Maroti, P.K.; Sharma, A. An extensive practical investigation of FPSO-based MPPT for grid integrated PV system under variable operating conditions with anti-islanding protection. *IEEE Syst. J.* **2018**, *13*, 1861–1871. [CrossRef]
20. Darvish, H.; Rahmani, S.; Maleki Sadeghi, A.; Emami Baghdadi, M.H. The ANFIS-PSO strategy as a novel method to predict interfacial tension of hydrocarbons and brine. *Pet. Sci. Technol.* **2018**, *36*, 654–659. [CrossRef]
21. Ramezani, M.; Li, S.; Golestan, S. Analysis and controller design for stand-alone VSIs in synchronous reference frame. *IET Power Electron.* **2017**, *10*, 1003–1012. [CrossRef]
22. Gonzalez, I.; Calderón, A.J.; Folgado, F.J. IoT real time system for monitoring lithium-ion battery long-term operation in microgrids. *J. Energy Storage* **2022**, *51*, 104596. [CrossRef]

23. Tremblay, O.; Dessaint, L.A. Experimental validation of a battery dynamic model for EV applications. *World Electr. Veh. J.* **2009**, *3*, 289–298. [CrossRef]

24. Adhikari, S.; Xu, Y.; Li, F.; Li, H.; Kueck, J.D.; Snyder, I.B.; Barker, T.J.; Hite, R. Utility-side voltage and PQ control with inverter-based photovoltaic systems. *IFAC Proc. Vol.* **2011**, *44*, 6110–6116. [CrossRef]

25. Naji Alhasnawi, B.; Jasim, B.H.; Esteban, M.D. A new robust energy management and control strategy for a hybrid microgrid system based on green energy. *Sustainability* **2020**, *12*, 5724. [CrossRef]

26. Chau, T.K.; Yu, S.S.; Fernando, T.; Iu, H.H.C.; Small, M. An investigation of the impact of PV penetration and BESS capacity on islanded microgrids–a small-signal based analytical approach. In Proceedings of the 2019 IEEE International Conference on Industrial Technology (ICIT), Melbourne, VIC, Australia, 13–15 February 2019; IEEE: Piscataway, NJ, USA, 2019; pp. 1679–1684.

27. Kafle, L.; Ni, Z.; Tonkoski, R.; Qiao, Q. Frequency control of isolated micro-grid using a droop control approach. In Proceedings of the 2016 IEEE International Conference on Electro Information Technology (EIT), Grand Forks, ND, USA, 19–21 May 2016; IEEE: Piscataway, NJ, USA, 2016; pp. 0771–0775.

28. Majumder, R.; Chaudhuri, B.; Ghosh, A.; Majumder, R.; Ledwich, G.; Zare, F. Improvement of stability and load sharing in an autonomous microgrid using supplementary droop control loop. *IEEE Trans. Power Syst.* **2009**, *25*, 796–808. [CrossRef]

29. Firdaus, A.; Mishra, S. A double derivative-based droop controller for improved power sharing in inverter based autonomous microgrid. In Proceedings of the 2018 IEEMA Engineer Infinite Conference (eTechNxT), New Delhi, India, 13–14 March 2018; IEEE: Piscataway, NJ, USA, 2018; pp. 1–6.

30. He, J.; Li, Y.W.; Blaabjerg, F. An enhanced islanding microgrid reactive power, imbalance power, and harmonic power sharing scheme. *IEEE Trans. Power Electron.* **2014**, *30*, 3389–3401. [CrossRef]

31. Zhong, Q.-C.; Hornik, T. Cascaded current–voltage control to improve the power quality for a grid-connected inverter with a local load. *IEEE Trans. Ind. Electron.* **2012**, *60*, 1344–1355. [CrossRef]

32. Marwali, M.N.; Keyhani, A. Control of distributed generation systems-Part I: Voltages and currents control. *IEEE Trans. Power Electron.* **2004**, *19*, 1541–1550. [CrossRef]

33. Giroux, P.; Tremblay, O.; Sybille, G.; Brunelle, P. Microgrid Dynamic Operation. 2021. Available online: https://www.mathworks.com/matlabcentral/fileexchange/93235-microgrid-dynamic-operation (accessed on 4 May 2023).